Eur J Nucl Med Mol Imaging (2011) 38 (Suppl 1):S10–S18
DOI 10.1007/s00259-011-1768-2

REVIEW ARTICLE

Quantitative imaging of ^{124}I and ^{86}Y with PET

Mark Lubberink · Hans Herzog

Received: 2 February 2011 / Accepted: 22 February 2011 / Published online: 12 April 2011

Abstract The quantitative accuracy and image quality of positron emission tomography (PET) measurements with ^{124}I and ^{86}Y is affected by the prompt emission of gamma radiation and positrons in their decays, as well as the higher energy of the emitted positrons compared to those emitted by ^{18}F. PET scanners cannot distinguish between true coincidences, involving two 511-keV annihilation photons, and coincidences involving one annihilation photon and a prompt gamma, if the energy of this prompt gamma is within the energy window of the scanner. The current review deals with a number of aspects of the challenge this poses for quantitative PET imaging. First, the effect of prompt gamma coincidences on quantitative accuracy of PET images is discussed and a number of suggested corrections are described. Then, the effect of prompt gamma coincidences and the increased singles count rates due to gamma radiation on the count rate performance of PET is addressed, as well as possible improvements based on modification of the scanner's energy windows. Finally, the effect of positron energy on spatial resolution and recovery is assessed. The methods presented in this overview aim to overcome the challenges associated with the decay characteristics of ^{124}I and ^{86}Y. Careful application of the presented correction methods can allow for quantitatively accurate images with improved image contrast.

M. Lubberink (✉)
Department of Medical Physics and PET Centre,
Uppsala University Hospital,
751 85 Uppsala, Sweden
e-mail: mark.lubberink@akademiska.se

H. Herzog
Institute of Neuroscience and Medicine - 4,
Forschungszentrum Jülich,
Jülich, Germany

Keywords PET · Positron emission tomography · ^{86}Y · ^{124}I · Quantitative imaging · Radionuclide therapy · Dosimetry

Introduction

Generally positron emission tomography (PET) is considered as a quantitative imaging modality which is able to measure the radioactivity concentration within the patient not just as count rates, but in absolute terms with the unit of becquerel per millilitre. This quantitative measurement is a prerequisite for calculating the radiation dose administered to target and healthy tissues in radionuclide therapy. The quantitative property of PET is based on positron emission and the subsequent annihilation process with the emission of a pair of photons in opposite directions with an energy of 511 keV each. Although the coincident measurement of a pair of annihilation photons by a ring of detectors surrounding the patient is disturbed by random and scattered (Fig. 2) coincidences as well as by events lost due to tissue attenuation, the related errors can be corrected sufficiently so that the final quantitation error is in the range of a few per cent. While this situation holds for the typical positron emitters ^{18}F or ^{11}C, it is no longer true for isotopes such as ^{124}I and ^{86}Y. These radionuclides do not only emit positrons, but also additional gamma radiation which may disturb quantitative PET imaging and image quality in a number of ways. Figure 1 shows simplified decay schemes of ^{124}I, ^{86}Y and, for comparison, ^{89}Zr and ^{18}F. The decay schemes of the nonstandard positron emitters include gamma radiation of different energies and abundances. This gamma radiation, also called prompt or cascade gamma radiation, is often emitted essentially simultaneously with positrons. The amount and the energy of the prompt gamma radiation is different for the various nonstandard positron emitters.

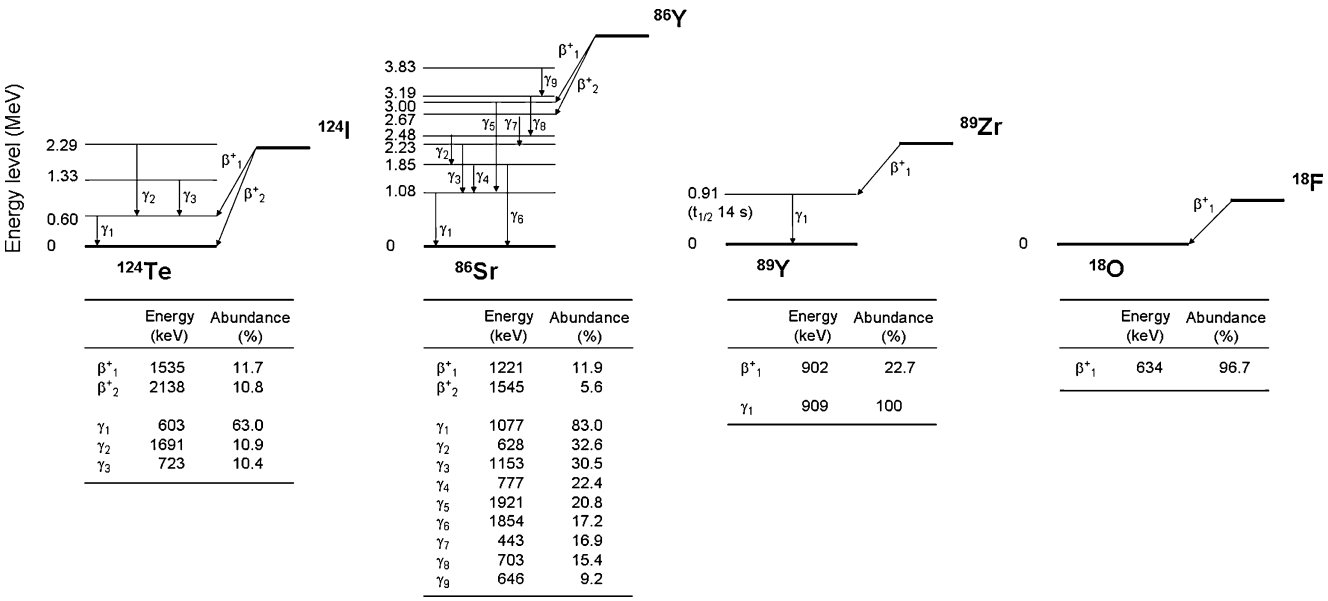

	Energy (keV)	Abundance (%)
β^+_1	1535	11.7
β^+_2	2138	10.8
γ_1	603	63.0
γ_2	1691	10.9
γ_3	723	10.4

	Energy (keV)	Abundance (%)
β^+_1	1221	11.9
β^+_2	1545	5.6
γ_1	1077	83.0
γ_2	628	32.6
γ_3	1153	30.5
γ_4	777	22.4
γ_5	1921	20.8
γ_6	1854	17.2
γ_7	443	16.9
γ_8	703	15.4
γ_9	646	9.2

	Energy (keV)	Abundance (%)
β^+_1	902	22.7
γ_1	909	100

	Energy (keV)	Abundance (%)
β^+_1	634	96.7

Fig. 1 Simplified decay schemes of ^{124}I, ^{86}Y, ^{89}Zr and, for comparison, the 'standard' PET isotope ^{18}F. Only radiation with abundance >5% is shown. Energy shown for positrons is maximum energy. Data based on [39]

In the decay of ^{124}I, with a positron abundance of approximately 23%, about 50% of all positrons (β^+_1 in Fig. 1) are emitted simultaneously with a 603-keV gamma photon (γ_1 in Fig. 1). In the case of ^{86}Y, on average about three photons are emitted per decay, compared to a positron abundance of 32%. All ^{86}Y positrons are emitted simultaneously with either a 1,077- or a 1,854-keV gamma photon (γ_1 and γ_6), and 628- and 443-keV photons are emitted in 33 and 17% of all decays, respectively. Furthermore, the energy of the positrons emitted by ^{124}I and ^{86}Y is higher than the positron energy of ^{18}F. This affects the spatial resolution of the PET images leading to decreased recovery and, consequently, underestimation of radioactivity concentrations in small structures [1].

Apart from ^{124}I and ^{86}Y as obvious analogues of therapeutic radionuclides, ^{89}Zr (half-life 78.4 h) is included here since it has been suggested as an analogue for ^{90}Y when labelling monoclonal antibodies [2]. ^{89}Zr has much preferred imaging properties compared to ^{86}Y. The aim of this chapter is to discuss the quantitation issues related to the use of ^{124}I and ^{86}Y and, additionally, ^{89}Zr with PET, as well as possible corrections and improvements.

Prompt or cascade gamma coincidences

Prompt or (cascade) gamma coincidences occur as coincidences of simultaneously emitted gamma photons with energies accepted within the energy discrimination window (e.g. 400–650 keV) with each other or with annihilation photons and cannot be distinguished from true coincidences, involving two annihilation photons. Detection of these essentially true coincidences therefore introduces a bias in the images which is not corrected for by the standard PET corrections [3–6] (Fig. 2). Since the directions of the gamma photons and the annihilation photons are not correlated, the gamma coincidences are distributed nearly uniformly within the PET field of view (FOV) causing a primarily flat background in the sinograms, as indicated in Fig. 3, and in the reconstructed images. This bias also results in degraded image contrast [4, 7].

In the case of ^{124}I, β^+_1 is always emitted simultaneously with a 603-keV photon whereas β^+_2 emission results directly in the ground state of ^{124}Te, which means that 52% of the positrons is emitted simultaneously with a prompt gamma. For ^{86}Y, the main two positrons are always emitted

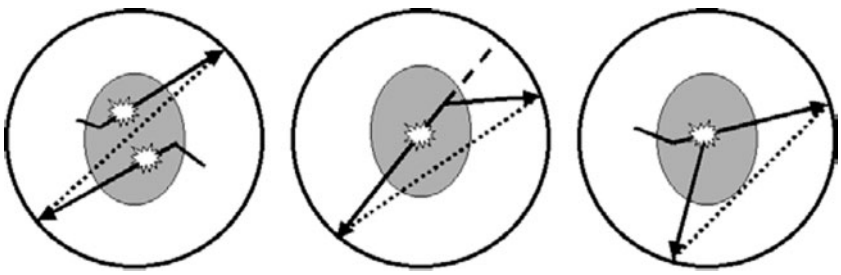

Fig. 2 Degrading effects in PET, from *left* to *right* random coincidences, scattered radiation and prompt gamma coincidences where one of the annihilation photons is detected in coincidence with a prompt gamma photon. Reprinted from [4] with permission from IOP Publishing

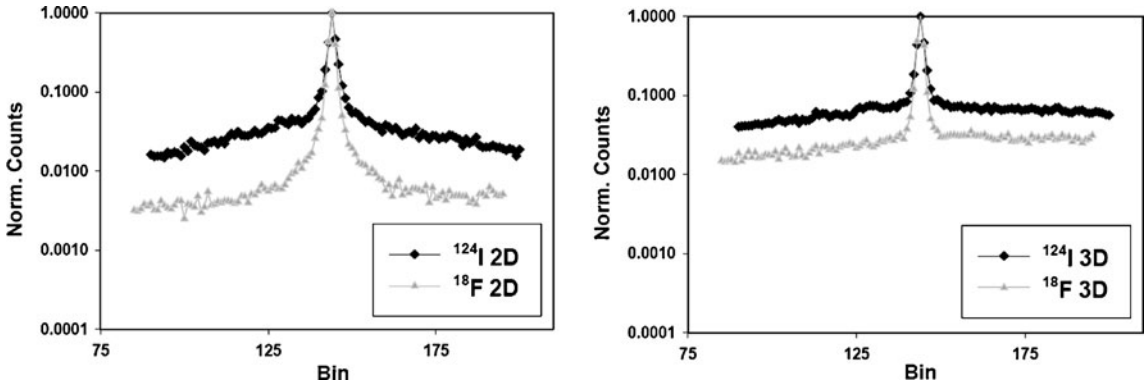

Fig. 3 Normalized line source profiles derived from sinograms of ^{124}I or ^{18}F line sources inside a cylindrical phantom filled with water. Reprinted from [10] with permission from Elsevier

simultaneously with at least two photons, and all other positrons are emitted simultaneously with at least one photon. Most of these photons have energies greater than 600 keV. Even if the primary energy of a prompt gamma is above the higher energy level of the energy discrimination window, the prompt gamma may be accepted after being scattered within the patient or septa and having lost part of its energy. For both isotopes, electron capture decays lead to multiple gamma photons emitted simultaneously, which might cause a so-called multiple coincidence. In addition, a multiple coincidence is recorded if a true coincidence is detected simultaneously with a prompt gamma. The probability of multiple coincidences is rather low, but increases with a larger spatial angle of the PET detectors. Such events are discarded in most PET scanners.

For ^{89}Zr, on the other hand, prompt gamma coincidences do not occur since the metastable 0.91 MeV level of ^{89}Zr has a half-life of 14 s [8], as shown in Fig. 1.

As illustrated in Fig. 3, which compares the background caused by ^{124}I with that of ^{18}F, the background is greater in 3-D PET than in 2-D where the septa limit the acceptance angle for photons not being within a plane perpendicular to the scanner's axis. Therefore, random and scattered coincidences as well as gamma coincidences are decreased. On the other hand, simulation studies have shown that the principle advantage of 2-D imaging is to some extent counterbalanced by an increase in the relative effect of prompt gamma radiation due to down-scatter of high energy photons in the septa [9].

Earlier generation PET scanners, such as the Scanditronix PC4096 WB (Scanditronix, Uppsala, Sweden), had very long and thick septa so that the recorded rate of gamma coincidences became very low despite possible down-scatter. The advantage of this kind of 2-D PET became obvious by the papers of Pentlow et al., Herzog et al. and Lubberink et al. [4, 10–13], and it can be concluded that early studies using the PC4096 WB scanner for quantitative imaging of nonstandard positron emitters provided valid results even without any corrections for prompt gamma coincidences.

The effect on quantitation due to the background caused by the gamma coincidences depends on the specific nonstandard positron emitter and on the specific tissue or target to be examined. In the case of ^{124}I and imaging of thyroid cancer, the radioactivity distribution is limited to a few foci, whereas the backgound is distributed across the entire image and thus contributes little to the activity concentration in a lesion. This situation is similar to that displayed in Fig. 3, where the ratio of counts measured at the maximum of a ^{124}I point source in water and of the

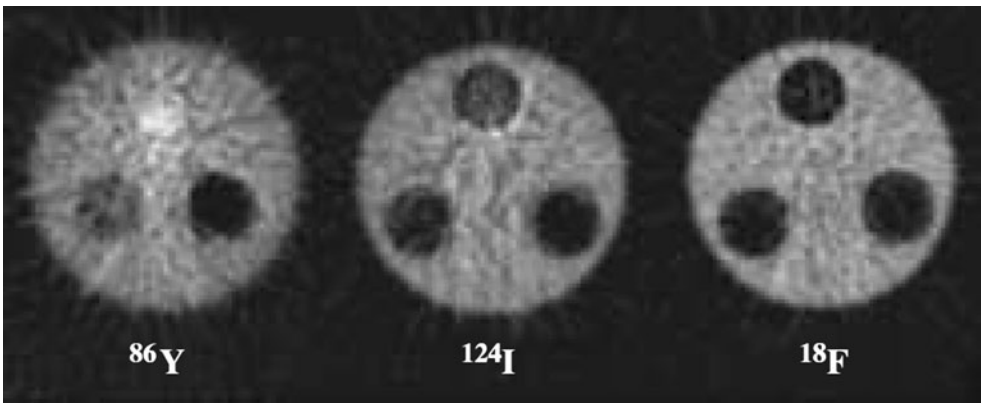

Fig. 4 Images of a NEMA 1994 phantom with cold Teflon (*top*), water (*left*) and air (*right*) inserts. The measurements were done with an ECAT Exact HR+ (Siemens/CTI, Knoxville, TN, USA) PET scanner in 3-D acquisition mode. There is a clear bias in the Teflon and water inserts for ^{86}Y and, to a lesser extent, for ^{124}I. Reprinted with permission from [16], ©2008 Edizione Minerva Medica

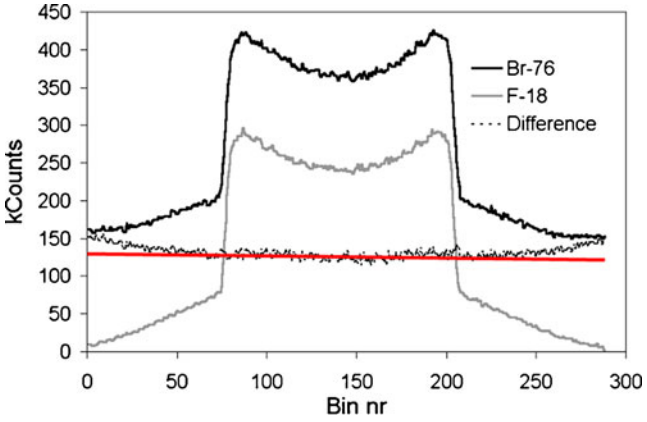

Fig. 5 Projections of a torso phantom filled with ^{76}Br and ^{18}F, along its short axis, as measured on an ECAT Exact HR+ scanner in 3-D mode. The decay scheme of ^{76}Br resembles that of ^{86}Y. The difference between both projections shows the contribution of gamma coincidences. The *red line* indicates the linear fit used to correct for prompt gamma coincidences, corresponding to 80% of the counts in the outermost bins. Adapted from [23]

background counts is more than 10:1. For labelled antibodies, however, the situation is different. Here, a lot of the radioactivity remains in the blood or is distributed to major organs. This effect may be considerable. Figure 4 illustrates the background found in a cold water rod which is located in a phantom homogeneously filled with ^{18}F, ^{124}I or ^{86}Y. The radioactivity concentration measured at the cold water rod relative to the surrounding radioactivity is 2% for ^{18}F, 14% for ^{124}I and 56% for ^{86}Y. Figure 4 also documents that considerably greater errors are found in bone regions which are simulated by the Teflon rod of the phantom. In this case, the radioactivity concentration measured at the Teflon rod relative to the surrounding radioactivity is 13% for ^{18}F, 44% for ^{124}I and 147% for ^{86}Y.

Correction

Several methods have been suggested to correct for the bias caused by prompt gamma coincidences. Firstly, subtraction of a uniform background [4, 14] or a linear background fitted to the sinogram data outside the object [4, 15] (shown for ^{76}Br in Fig. 5) has been suggested. In 2-D mode, the assumption can be made that the outermost bins in the sinogram contain only prompt gamma coincidences, since scatter is negligible in these bins. Depending on the size of the imaged object, however, this assumption may be wrong, and especially in 3-D acquisition mode there is a considerable amount of scatter in the edge bins. Herzog et al. [16] found that 75% of the background had to be subtracted for ^{86}Y to obtain similar residual correction errors in a cylindrical phantom with cold inserts as for ^{18}F. Buchholz et al. compared phantom measurements with and without a uniform background subtraction for different scanners [17]. An example of the effect of subtraction of a uniform background on ^{86}Y patient data is shown in Fig. 6. Although this subtraction gives a good first approximation for cylindrical objects in the centre of the FOV, the assumption that the background caused by prompt gamma coincidences is linear is generally not valid, as clearly shown in Figs. 5 and 8. Therefore, Kull et al. [15] used a second-order series expansion to describe the shape of the background for 2-D scans with ^{86}Y, where they determined the second-order term using a measurement with a body phantom and the linear portion of the background by fitting to the sinogram tails of the individual patient, and also included a recalibration of the scanner based on the trues to singles ratio.

A convolution subtraction algorithm based on the method suggested by Bergström et al. in the early 1980s

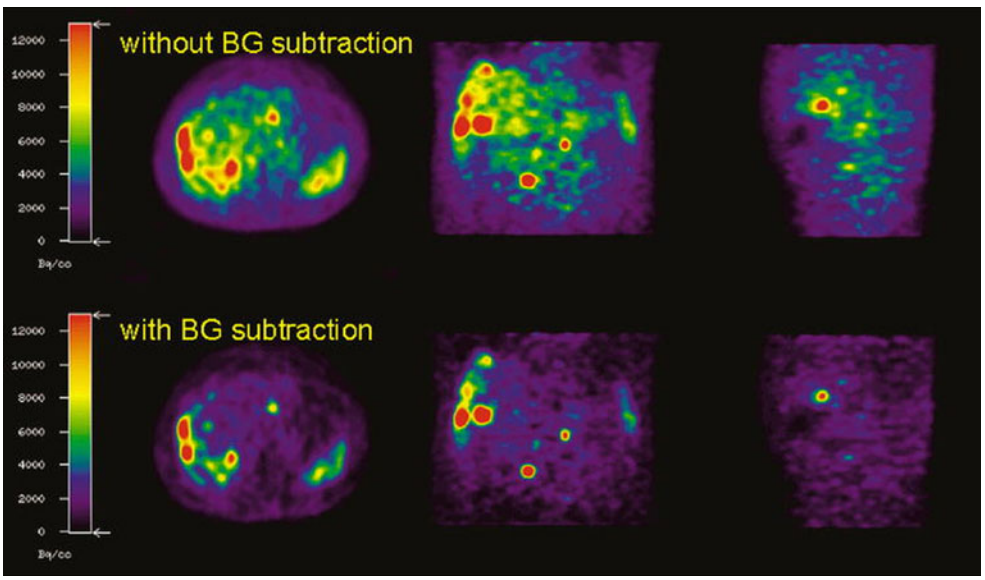

Fig. 6 ^{86}Y-DOTATOC images as measured with the ECAT Exact in 2-D mode, without (*top row*) and with (*bottom row*) subtraction of a uniform sinogram background. The corrected image shows a lower background in the liver and a considerable reduction of radioactivity concentration in the spine. Reprinted from Fig. 4 in [17] with kind permission from Springer Science+Business Media

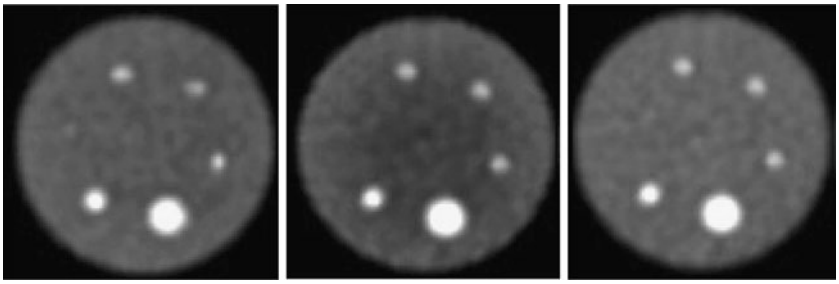

Fig. 7 Images of a 20-cm diameter phantom containing one 3-cm, one 1.5-cm and three 1-cm diameter spheres. From *left* to *right*: ^{18}F, ^{124}I without offset correction and ^{124}I with offset correction in the scaling of the scatter estimate. Reprinted with permission from [22], ©2009 IEEE

for correction for scattered radiation [18] was described by Beattie et al. [6]. This method does take patient-specific variations into account, but has only been described for 2-D acquisitions. Walrand et al. [5] used a patient-dependent correction method based on sinogram tail fitting using an ^{86}Y point spread function library, showing promising results. A geometrical correction was suggested by Schweizer and von Busch [19], calculating the contribution of prompt gamma coincidences of a number of source points to each line of response.

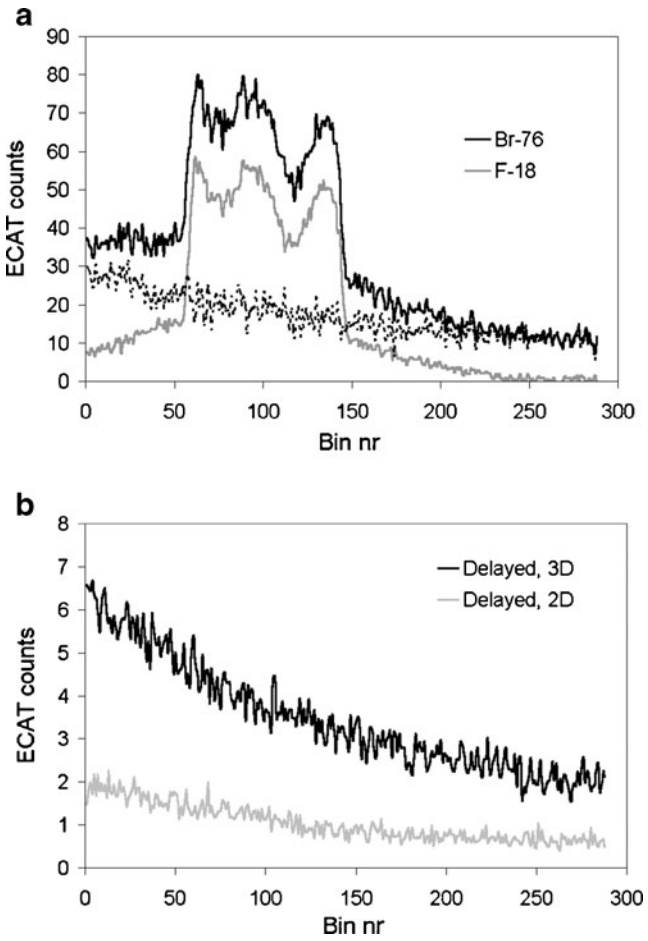

Fig. 8 Projections of a 10-cm off-centre cylindrical phantom with cold inserts filled with ^{76}Br (*solid black line*) and ^{18}F (*solid grey line*) as well as the prompt gamma contribution for ^{76}Br (*dashed line*) as measured with an ECAT Exact HR+ in 3-D mode (**a**) and corresponding delayed coincidence projections (**b**). Shapes of delayed coincidence and prompt gamma coincidence projections are approximately similar. Reprinted from [23]

The single-scatter simulation scatter correction applied on all last generation PET(/CT) scanners [20] usually includes a scaling to match the estimated scatter contribution to the actual events measured just outside the body. If this scaling includes both a multiplicative as well as an additive factor, it implicitly performs a crude correction for a uniform bias caused by prompt gamma coincidences as well. This has been shown by Surti et al. for ^{124}I on a Gemini PET/CT scanner (Philips Healthcare, Cleveland, OH, USA) [21, 22] (Fig. 7). As Fig. 7 also shows, using only a multiplicative factor leads to overcorrection in the centre of the image.

Finally, it has been shown that the distribution of prompt gamma coincidences matches the distribution of random coincidences rather well [23] (Fig. 8). Therefore, a correction method involving subtraction of a scaled randoms sinogram could be an accurate correction for prompt gamma coincidences [23], possibly incorporated into the single-scatter simulation. This method has been realized by Watson et al. and Hayden et al. [24, 25] for cardiac studies with the nonstandard positron emitter ^{82}Rb, which emits a 777-keV prompt gamma together with positrons in only 14% of decays and has, so far, not been implemented for ^{124}I or ^{86}Y.

Count rate performance

The increased singles rate due to gamma radiation leads to increased random coincidence rates and, consequently, reduced noise equivalent count (NEC) rates [26]. The increased random rate can be accurately corrected for using the standard delayed window method, but correction for a larger random fraction increases image noise. Figure 9 shows NEC rates for ^{124}I and ^{11}C as measured using a cylindrical phantom. To calculate these NEC rates, the scatter fraction for ^{11}C was computed according to a method described by de Jong et al. [27]. The total (scatter + prompt gamma) background was measured in a similar way for ^{124}I as for ^{11}C, and the prompt gamma

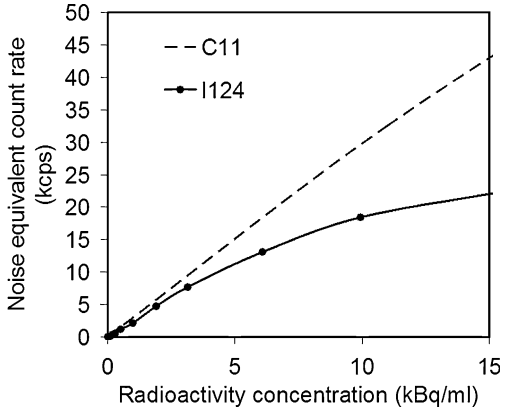

Fig. 9 NEC rates for a 20-cm diameter phantom filled with ^{124}I (*solid line*) and ^{11}C (*dashed line*) for the Gemini TF PET/CT scanner. Data for ^{11}C were based on Surti et al. [40] with radioactivity concentrations divided by 0.225 to account for the difference in positron abundance between ^{124}I and ^{11}C [31]

contribution to this background was estimated assuming identical scatter fractions for ^{11}C and ^{124}I. The NEC rate is then described by:

$$\mathrm{NEC} = \frac{\mathrm{T}^2}{\mathrm{T} + \mathrm{S} + \mathrm{G} + 2\mathrm{D}} \quad (1)$$

Here, *T* are the true coincidences, *S* and *G* are the number of scattered and prompt gamma coincidences, respectively, and *D* is the number of delayed coincidences.

For ^{124}I, and even more so for ^{86}Y, the fraction of detected photons with energy outside the scanner's energy window increases considerably compared to positron-only emitters. Rejection of photons outside the energy window does contribute to dead time, but these photons are, on most scanners, not counted in the singles rate. Since the dead time correction is usually implemented as a function of singles rate, it may become inaccurate [3, 15, 28, 29]. This effect has previously been shown for ^{86}Y [15], ^{124}I [28] as well as for ^{76}Br [29], which has a decay scheme somewhere in between that of ^{124}I and ^{86}Y in terms of the number of emitted prompt gamma photons.

Energy window

One option to improve image quality for isotopes emitting high-energy gamma radiation besides positrons may be the use of a narrower energy window, which reduces random coincidence rates involving higher-energy photons, such as the 603-keV photon emitted by ^{124}I [7, 30] (Figs. 10 and 11). Furthermore, the amount of scattered higher-energy gamma photons which may coincide with annihilation photons will be decreased. Gregory et al. found an increase in NEC rates of 48% for ^{124}I when changing the energy window from 409–665 keV to 455–588 keV on a Gemini Dual GS PET/CT scanner [28]. Due to its higher standard lower level discriminator, a more limited improvement was found for the Gemini TF scanner when changing the energy window from 440–665 keV to 440–560 keV [31]. In addition to a different energy window, a narrower coincidence window decreases random coincidence rates which is relatively of more importance for ^{124}I and ^{86}Y than for ^{18}F. Use of a narrower energy window, however, may increase the inaccuracy of dead time corrections as described in the previous paragraph, and energy window-specific scanner normalization may be required.

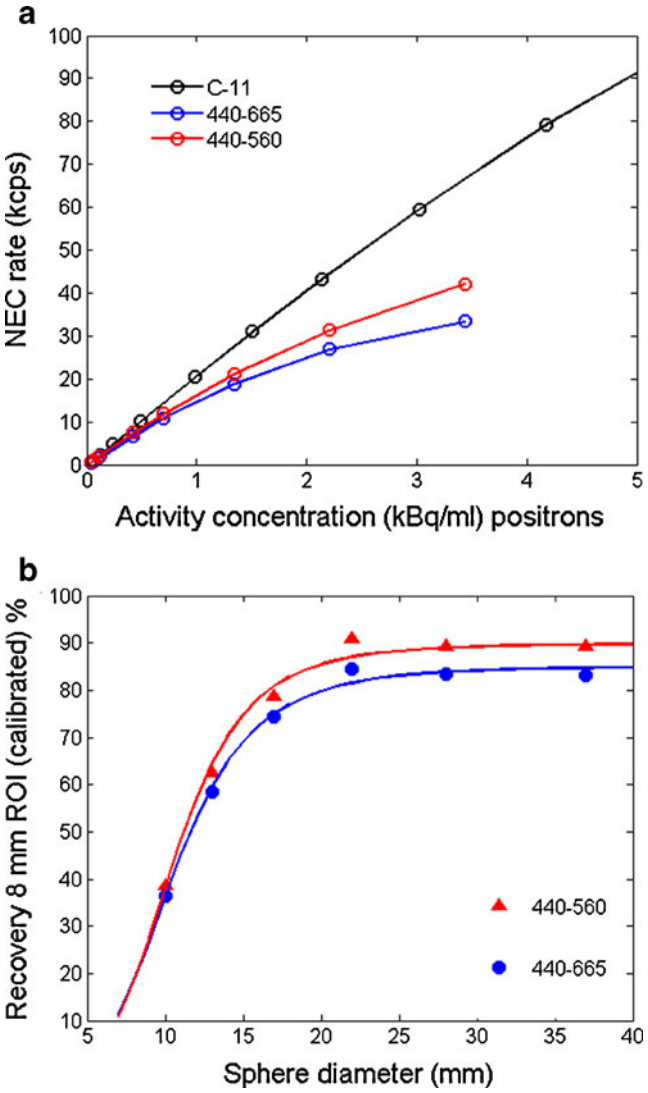

Fig. 10 **a** NEC rates, which are a measure of the signal to noise ratio, of the Gemini TF-64 with ^{11}C using the standard 440–665 keV energy window (*black*), for ^{124}I using this same window (*blue*) and for ^{124}I using a narrow 440–560 keV window (*red*). Activity concentrations were normalized for positron abundance. **b** Improvement in recovery of ^{124}I using the narrower energy window [31]

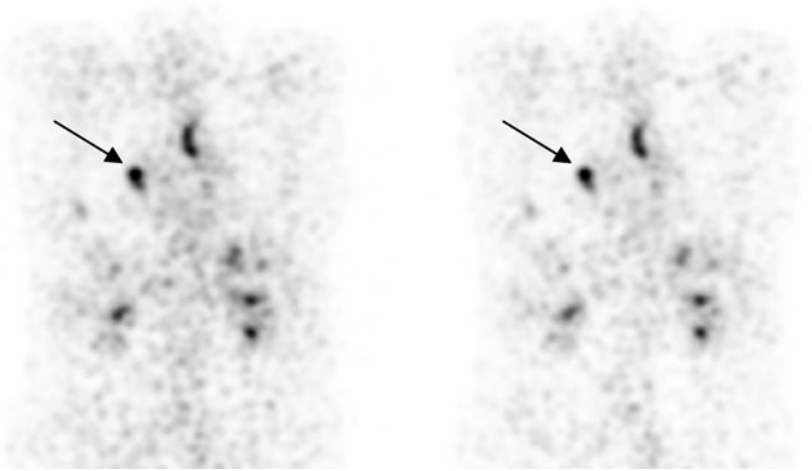

Fig. 11 PET images of a patient with metastatic thyroid cancer at 24 h after administration of 37 MBq ^{124}I acquired on a Gemini TF-64 PET/CT scanner (**a**) 440–665 keV and (**b**) 440–560 keV energy window. The narrower energy window results in a 15% improvement in image contrast in the largest metastasis (*arrow*) due to the decreased image background [31]

Resolution and recovery

One of the parameters influencing the accuracy of quantitation is image resolution. The lower the image resolution is, the greater is the partial volume effect which compromises the analysis of small structures. As a first approximation, the image resolution of PET can be estimated by the following equation:

$$r = 1.25\sqrt{\left(\frac{d}{2}\right)^2 + (0.0022 \cdot D)^2 + R^2 + b^2} \qquad (2)$$

where the image resolution r is expressed as full-width at half-maximum (FWHM), d is the detector width, D is the detector ring diameter and R is the effective positron range [32]. The factor b equals 0 for detectors individually coupled to photomultiplier tubes and 2 for a block detector design.

This equation takes into account the positron energy as an important factor influencing the image resolution. Both ^{86}Y and ^{124}I emit positrons with different energies with average energies ranging from 550 to 898 keV and from 686 to 973 keV, respectively [33]. For comparison, ^{18}F emits positrons with mean energy of 250 keV, ^{89}Zr with 389 keV, ^{15}O with 735 keV and ^{68}Ga (mainly) with 836 keV. Thus, the positron ranges given in the literature for ^{15}O and ^{68}Ga (2.0 and 2.2 mm [34]) can be regarded as appropriate estimates for the mean positron ranges of ^{86}Y and ^{124}I, respectively. The mean positron range of ^{18}F is 0.64 mm. The consequences of the greater positron ranges of ^{86}Y and ^{124}I can be estimated with Eq. 2 and are summarized in Table 1 for typical design parameters of human and small animal PET.

Table 1 Theoretical spatial resolution (mm)

	Human PET d=4 mm, D=800 mm, b=2	Animal PET d=1.5 mm, D=150 mm, b=0
^{18}F	4.2	1.3
^{124}I	5.0	2.9
^{86}Y	4.9	2.7

Thus, for small animal PET the effect of high positron range is more severe than for human whole-body PET, both in the relative and absolute sense. Pentlow et al. evaluated the resolution of ^{124}I using phantoms containing hot spheres in a number of different scanners [11, 12], but did not report actual resolution values. Herzog et al. [10] measured an image resolution of 6.1 mm with ^{124}I and of 5.1 mm with ^{18}F in a line source centrally located in an HR + scanner and reconstructed with filtered backprojection and a Shepp filter of 2.5 mm. Vandenberghe [30] examined simulated line sources filled with ^{18}F, ^{86}Y or ^{124}I and placed centrally in an Allegro PET scanner (Philips Healthcare, Cleveland, OH, USA). The line spread functions showed FWHM values of 4.8, 5.7 and 6.1 mm, respectively.

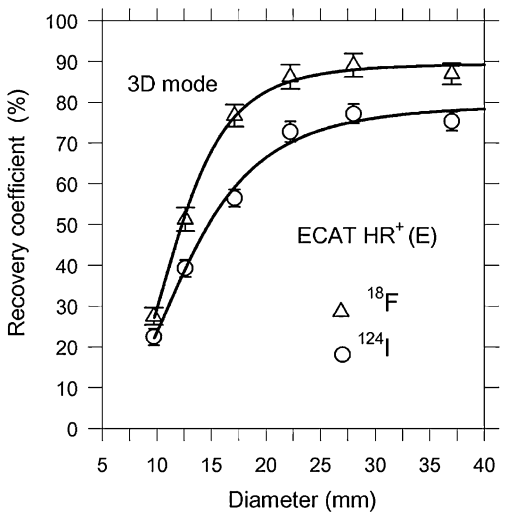

Fig. 12 Recovery for ^{124}I and ^{18}F as measured with an ECAT Exact HR+ scanner in 3-D mode. Reprinted from Fig. 2 in [38] with kind permission from Springer Science+Business Media

Comparative resolution measurements were performed by González Trotter et al. [35] using line sources filled with either ^{18}F or ^{124}I and placed in the centre of a Discovery LS PET/CT scanner (GE Healthcare, Milwaukee, WI, USA) operated in 2-D mode. After reconstruction with filtered backprojection using a Gaussian filter of 7 mm the measured resolution was 8.71 and 9.74 mm, respectively. Bading et al. [36] examined the degradation of image resolution, when ^{124}I was used comparatively with ^{18}F in a microPET R4 small animal scanner (Concorde/Siemens, Knoxville, TN, USA). In the scanner's centre the FWHM was 2.3 mm for ^{124}I and 1.9 mm for ^{18}F. Using a Discovery STE PET/CT scanner Zhu and El Fakhri [37] studied the spatial resolution of ^{18}F and ^{86}Y with a line source placed centrally in air and reported values of 5.56 and 6.06 mm. Gregory et al. reported a resolution degradation of 0.7 mm for ^{124}I compared to ^{18}F for the Gemini Dual GS PET/CT scanner [28]. Although the numbers just summarized differ depending on the scanner and reconstruction method applied in the respective studies, the effect of the higher positron energies of ^{86}Y and ^{124}I is obvious: concordantly the image resolution is reported to be 0.5–1 mm inferior to that when using ^{18}F. Considering the small increase in positron energy between ^{18}F and ^{89}Zr, only a minor degradation in resolution of about 0.1 mm is expected for ^{89}Zr.

The effect of this degradation of image resolution for ^{124}I on recovery, that is, the ability of the PET scanner to quantify the radioactivity concentration in small structures, was measured extensively by Jentzen et al. [38] (Fig. 12). Recovery for ^{124}I was considerably worse than for ^{124}I, even for spheres as large as 37 mm in diameter. This has to be accounted for when quantifying tumour uptake of ^{124}I for dose estimations in thyroid cancer therapy, and the authors conclude that recovery correction is mandatory for ^{124}I, even for large structures.

Summary

The decay characteristics of ^{124}I and ^{86}Y set a challenge to quantitative imaging of these isotopes. The methods presented in this overview aim to overcome this as well as to improve image quality, and careful application of presented correction methods can allow for quantitatively accurate images with improved image contrast.

Acknowledgement The authors thank Dr. Marc Huisman (VU University Medical Center, Amsterdam) for critical reading of the manuscript.

References

1. Jentzen W. Experimental investigation of factors affecting the absolute recovery coefficients in iodine-124 PET lesion imaging. Phys Med Biol 2010;55(8):2365–98.
2. Perk LR, Visser GW, Vosjan MJ, Stigter-van Walsum M, Tijink BM, Leemans CR, et al. (89)Zr as a PET surrogate radioisotope for scouting biodistribution of the therapeutic radiometals (90)Y and (177)Lu in tumor-bearing nude mice after coupling to the internalizing antibody cetuximab. J Nucl Med 2005;46(11):1898–906.
3. Martin CC, Christian BT, Satter MR, Nickerson LDH, Nickles RJ. Quantitative PET with positron emitters that emit prompt gamma rays. IEEE Trans Med Imaging 1995;14(4):681–7.
4. Lubberink M, Schneider H, Bergström M, Lundqvist H. Quantitative imaging and correction for cascade gamma radiation of 76Br with 2D and 3D PET. Phys Med Biol 2002;47 (19):3519–34.
5. Walrand S, Jamar F, Mathieu I, De Camps J, Lonneux M, Sibomana M, et al. Quantitation in PET using isotopes emitting prompt single gammas: application to yttrium-86. Eur J Nucl Med Mol Imaging 2003;30(3):354–61.
6. Beattie BJ, Finn RD, Rowland DJ, Pentlow KS. Quantitative imaging of bromine-76 and yttrium-86 with PET: a method for the removal of spurious activity introduced by cascade gamma rays. Med Phys 2003;30(9):2410–23.
7. Lubberink M, van Schie A, de Jong HW, van Dongen GA, Teule GJ. Acquisition settings for PET of 124I administered simultaneously with therapeutic amounts of 131I. J Nucl Med 2006;47 (8):1375–81.
8. Monaro S, Vingiani GB, van Lieshout R. Aspects of decay of 27Mg and of 89Zr. Physica 1961;27(10):985–993.
9. Kolthammer JA, Salem N, Fiedler K, Gagnon D. Downscatter contamination from high-energy photons of 124I in 2D and 3D PET. IEEE Nucl Sci Symp Conf Rec 2004;6:3629–33.
10. Herzog H, Tellmann L, Qaim SM, Spellerberg S, Schmid A, Coenen HH. PET quantitation and imaging of the non-pure positron-emitting iodine isotope 124I. Appl Radiat Isot 2002;56 (5):673–9.
11. Pentlow KS, Graham MC, Lambrecht RM, Cheung NK, Larson SM. Quantitative imaging of I-124 using positron emission tomography with applications to radioimmunodiagnosis and radioimmunotherapy. Med Phys 1991;18(3):357–66.
12. Pentlow KS, Graham MC, Lambrecht RM, Daghighian F, Bacharach SL, Bendriem B, et al. Quantitative imaging of iodine-124 with PET. J Nucl Med 1996;37(9):1557–62.
13. Lubberink M, Lundqvist H, Westlin JE, Tolmachev V, Schneider H, Lövqvist A, et al. Positron emission tomography and radioimmunotargeting–aspects of quantification and dosimetry. Acta Oncol 1999;38(3):343–9.
14. Pentlow KS, Finn RD, Larson SM, Erdi YE, Beattie BJ, Humm JL. Quantitative imaging of yttrium-86 with PET. The occurrence and correction of anomalous apparent activity in high density regions. Clin Positron Imaging 2000;3(3):85–90.
15. Kull T, Ruckgaber J, Weller R, Reske S, Glatting G. Quantitative imaging of yttrium-86 PET with the ECAT EXACT HR+ in 2D mode. Cancer Biother Radiopharm 2004;19(4):482–90.
16. Herzog H, Tellmann L, Scholten B, Coenen HH, Qaim SM. PET imaging problems with the non-standard positron emitters yttrium-86 and iodine-124. Q J Nucl Med Mol Imaging 2008;52 (2):159–65.
17. Buchholz HG, Herzog H, Förster GJ, Reber H, Nickel O, Rösch F, et al. PET imaging with yttrium-86: comparison of phantom measurements acquired with different PET scanners before and

after applying background subtraction. Eur J Nucl Med Mol Imaging 2003;30(5):716–20.
18. Bergström M, Eriksson L, Bohm C, Blomqvist G, Litton J. Correction for scattered radiation in a ring detector positron camera by integral transformation of the projections. J Comput Assist Tomogr 1983;7(1):42–50.
19. Schweizer B, von Busch H. Koninklijke Philips Electronics, assignee. Dirty isotope PET reconstruction. United States patent 20090057561. 2009.
20. Watson CC. New, faster, image-based scatter correction for 3D PET. IEEE Trans Nucl Sci 2000;47(4):1587–94.
21. Gregory R, Partridge M, Flux GD. Assessment of cascade correction methods for quantitative 124I PET imaging. Eur J Nucl Med Mol Imaging 2009;36:OP066.
22. Surti S, Scheuermann R, Karp JS. Correction technique for cascade gammas in I-124 imaging on a fully-3D, time-of-flight PET scanner. IEEE Trans Nucl Sci 2009;56(3):653–60.
23. Lubberink M. Quantitative imaging with PET - performance and applications of 76Br, 52Fe, 110mIn and 134La. Uppsala: Acta Universitatis Upsaliensis. Comprehensive summaries of Uppsala dissertations from the faculty of medicine 2001;1034.
24. Watson CC, Hayden C, Casey ME, Hamill J, Bendriem B. Prompt gamma correction for improved quantification in 82Rb PET. J Nucl Med 2008;49:64P.
25. Hayden CH, Casey ME, Watson CC. Siemens Medical Solutions, assignee. Prompt gamma correction for non-standard isotopes in a PET scanner. United States patent 20080283758. 2008.
26. Strother SC, Casey ME, Hoffman EJ. Measuring PET scanner sensitivity: relating count rates to image signal-to-noise ratios using noise equivalent counts. IEEE Trans Nucl Sci 1990;37 (2):783–8.
27. de Jong HW, Lubberink M, Watabe H, Iida H, Lammertsma AA. A method to measure PET scatter fractions for daily quality control. Med Phys 2009;36(10):4609–15.
28. Gregory RA, Hooker CA, Partridge M, Flux GD. Optimization and assessment of quantitative 124I imaging on a Philips Gemini dual GS PET/CT system. Eur J Nucl Med Mol Imaging 2009;36 (7):1037–48.
29. Lubberink M, Schneider H, Bergström M, Lundqvist H. Count rate characteristics of PET with bromine-76. Eur J Nucl Med 2001;28(8):1008.
30. Vandenberghe S. Three-dimensional positron emission tomography imaging with 124I and 86Y. Nucl Med Commun 2006;27 (3):237–45.
31. Bol K. Performance, quality and optimization of 124I imaged with the Phillips GEMINI TF PET/CT [Master's thesis]. Amsterdam: VU University; 2009.
32. Moses WW, Derenzo SE. Empirical observation of resolution degradation in positron emission tomographs utilizing block detectors. J Nucl Med 1993;34:101P.
33. ICRP Publication 38: Radionuclide transformations: energy and intensity of emissions. Ottawa: International Commission on Radiological Protection; 1983.
34. Evans RD. The atomic nucleus. New York: McGraw-Hill; 1972.
35. González Trotter DE, Manjeshwar RM, Doss M, Shaller C, Robinson MK, Tandon R, et al. Quantitation of small-animal (124)I activity distributions using a clinical PET/CT scanner. J Nucl Med 2004;45(7):1237–44.
36. Bading JR, Hörling M, Williams LE, Colcher D, Raubitschek A, Strand SE. Quantitative serial imaging of an 124I anti-CEA monoclonal antibody in tumor-bearing mice. Cancer Biother Radiopharm 2008;23(4):399–409.
37. Zhu X, El Fakhri G. Monte Carlo modeling of cascade gamma rays in (86)Y PET imaging: preliminary results. Phys Med Biol 2009;54(13):4181–93.
38. Jentzen W, Weise R, Kupferschläger J, Freudenberg L, Brandau W, Bares R, et al. Iodine-124 PET dosimetry in differentiated thyroid cancer: recovery coefficient in 2D and 3D modes for PET (/CT) systems. Eur J Nucl Med Mol Imaging 2008;35(3):611–23.
39. Chu SYF, Ekström LP, Firestone RB. WWW table of radioactive isotopes, database version 2/28/1999 from http://nucleardata.nuclear.lu.se/nucleardata/toi/. 1999.
40. Surti S, Kuhn A, Werner ME, Perkins AE, Kolthammer J, Karp JS. Performance of Philips Gemini TF PET/CT scanner with special consideration for its time-of-flight imaging capabilities. J Nucl Med 2007;48(3):471–80.